Comparative investigation on macroscopic and microscopic characteristics of impingement spray of gasoline and ethanol from a GDI injector under injection pressure up to 50 MPa

Xiang Li [a, b, *], Dayou Li [a], Pavlos Dimitriou [c], Tahmina Ajmal [a], Abdel Aitouche [d, e], Raouf Mobasheri [d, e],

Oyuna Rybdylova [f], Yiqiang Pei [b, *], Zhijun Peng [g, *]

[a] School of Computer Science and Technology, University of Bedfordshire, Luton, UK

[b] State Key Laboratory of Engines, Tianjin University, Tianjin, China

[c] Guangdong Technion-Israel Institute of Technology, Shantou, Guangdong, China

[d] Univ. Lille, CNRS, Centrale Lille, UMR 9189 - CRIStAL - Centre de Recherche en Informatique Signal et Automatique de Lille, F-59000 Lille, France

[e] Junia, Smart Systems and Energies, F-59000 Lille, France

[f] Advanced Engineering Centre, School of Architecture, Technology and Engineering, University of Brighton, Brighton, UK

[g] School of Engineering, University of Lincoln, Lincoln, UK

*Corresponding author:

Xiang Li, School of Computer Science and Technology, University of Bedfordshire, Luton, LU1 3JU, UK

Email: xiang.li@beds.ac.uk

Yiqiang Pei, State Key Laboratory of Engines, Tianjin University, Tianjin, 300072, China.

Email: peiyq@tju.edu.cn

Zhijun Peng, School of Engineering, University of Lincoln, Lincoln, LN6 7TS, UK

Email: jpeng@lincoln.ac.uk

Abstract

Particulate Matter (PM) emissions from passenger vehicles have attracted considerable interest over the last decade. In order to reduce PM emissions, improving maximum injection pressure has been a developing trend for new generation GDI engines. However, comparing gasoline and ethanol impingement spray characteristics from a GDI injector under high injection pressure is still unclear. In this paper, a comparative investigation on both the macroscopic and microscopic characteristics of impingement spray from a GDI injector fuelled with gasoline and ethanol was performed under injection pressure up to 50 MPa, providing new findings to promote a more homogeneous air-fuel mixture and reduce PM emissions. The experimental results show that under the same P_I (injection pressure), rebound height of gasoline impingement spray is a bit higher than ethanol. A_S (spray area) of gasoline is slightly higher than ethanol under P_I = 10 MPa. However, under P_I = 30 MPa and P_I = 50 MPa, A_S of gasoline is gradually exceeded by that of ethanol as time progresses. By increasing P_I to 50 MPa, the difference in D_N (diffusion distance of the near side) between gasoline and ethanol is greatly reduced, meantime D_F (diffusion distance of the far side) becomes weaker than ethanol. For both gasoline and ethanol, with the increase P_I from 10 MPa to 50 MPa, V_N (average normal component of droplet velocity) and V_T (average tangential component of droplet velocity) of incident droplets increase by around 1 m/s. Meantime, there is a slight decrease in the absolute value of V_N and V_T of reflected droplets. D_{SMD} (Sauter mean diameter of droplets) presents a significant decreasing trend with the increase of P_I. Besides, a smaller D_{SMD} can be seen for the gasoline impingement spray compared to ethanol under the same P_I.

1. Introduction

As one anthropogenic aerosol in the ecosystem, Particulate Matter (PM) emitted by passenger vehicles has been a prominent uncertainty factor of climate change, owing to its influences on the incoming solar radiation and outgoing thermal radiation [1][2]. Moreover, regarding the impacts on human health, fine PM could penetrate into the alveoli and blood, potentially leading to some respiratory and cardiovascular diseases [3]. Hence, PM emitted by passenger vehicles has attracted considerable interest worldwide. Battery Electric Vehicle (BEV) and Fuel Cell Electric Vehicle (FCEV) are proposed as two major effective technologies. But their market shares are much lower than that of Internal Combustion Engine (ICE) vehicles, due to some drawbacks, such as price performance, recharging facilities, recharging time and cruising range [4][5].

Regarding the powertrain system of ICE vehicles, owing to the benefits for engine thermal efficiency, Gasoline Direct Injection (GDI) engine has been the most popular choice instead of Port Fuel Injection (PFI) over the last few decades [6-11]. However, compared to PFI engines, the relatively high PM emissions from GDI engines become worthy of more attention, particularly the Euro 6c standard released in 2017 further restricted the PM number of GDI-powered vehicles from 6×10^{12} #/km to 6×10^{11} #/km [12][13][14].

The PM emission level of GDI engine is generally influenced by operating parameters, such as air-fuel ratio, spark timing, Exhaust Gas Recirculation (EGR), fuel injection timing and injection pressure. In order to reduce PM emissions, improving maximum injection pressure has been a

developing trend for new generation GDI engines in recent years [15]. Hence, some researchers have

commenced investigations related to GDI injector under the conditions of high injection pressure

equal to or greater than 30 MPa [16-25].

Husted et al. [16] experimentally investigated fuel economy with varying injection pressure from

10 MPa to 40 MPa. It was found that increasing fuel pressure is good for the fuel economy of GDI

engine, but the benefit is not obvious due to the growth of fuel consumption required by fuel pump.

Park et al. [17][18] studied the effects of injection pressure up to 50 MPa on combustion and emission

characteristics of a GDI engine. It was confirmed that increasing injection pressure could

considerably reduce gaseous and PM emissions. The maximum reduction in PM number,

hydrocarbon and nitrogen emissions can be up to 93.6%, 34.5% and 35.6%, respectively. Lou et al.

[19] demonstrated that with the increase of injection pressure from 35 MPa to 50 MPa, the proportion

of PM with a diameter below 23 nm is increased to more than 40% of total PM. Li et al. [20] evaluated

the macroscopic characteristics of ethanol spray from a GDI injector under injection pressure up to

50 MPa, by analysing spray development stages, cone angle, penetration, area and irregular ratio. Luo

et al. [21][22] studied the microscopic characteristics of near-nozzle spray and the impinging spray

from a GDI injector fuelled with surrogate fuels (n-heptane, toluene) with injection pressure up to 30

MPa. It indicated that the number of droplets with a diameter above 20 μm could be significantly

decreased by increasing injection pressure from 10 MPa to 30 MPa. Luo et al. [23] also carefully

analysed the effects of iso-octane spray characteristics under cross-flow conditions with an injection

of up to 35 MPa. It was found that with the increase of fuel injection pressure, both the spray

horizontal penetration and area distributions could become uniform. Using experiment and simulation

methods, Montanaro et al. [24][25] studied the effects of ultra-high injection pressure up to 100 MPa

88   on the spray morphology. It indicated that by increasing injection pressure from 40 MPa to 100 Mpa,

89   the spray cone angle has a slight increase of 2 degrees.

90   As mentioned above, regarding the studies related to GDI injector under high injection pressure

91   equal to or greater than 30 MPa, most previous researchers focused on GDI engine performance and

92   spray characteristics. Few studies have investigated the effects of high injection pressure on

93   impingement spray from a GDI injector. Furthermore, no investigation has systematically compared

94   gasoline and ethanol impingement spray from a GDI injector under high injection pressure. Besides,

95   biofuels have been a promising alternative and a hotspot, which have attracted great interest in the

96   research domain of ICE [26-32]. Particularly, owing to high content of oxygen, ethanol addition into

97   engine combustion process could help reduce PM emissions, which has become a popular solution to

98   achieve low-carbon emissions as the concern for the climate increased in recent years [28][29][30].

99   Hence, this paper aims to initially develop a theoretical framework for macroscopic and

100   microscopic characteristics of impingement spray from a GDI injector fuelled under injection

101   pressure up to 50 MPa, which is helpful to form a more homogeneous air-fuel mixture in GDI engines.

102   Moreover, a comparison between gasoline and ethanol impingement spray characteristics was

103   explored to provide new scientific perspectives and valuable references for further experimental and

104   simulation studies.

105   **2.   Experimental setup and method**

106   *2.1. Experimental setup and procedures of macroscopic spray characteristics*

107   The GDI injector used in this investigation is from a dual-injection Spark Ignition (SI) engine. As

108   the orifice geometry and spray sketch presented in Fig. 1, the injector has five holes with a diameter

109   of 0.174 mm. In this investigation, spray jets are numbered as jets "1" to "5". The utilised fuels are

110   commercial gasoline and absolute ethanol, which properties are listed in Table 1. Regarding the

111   effects of fuel properties in the utilisation of common GDI engines, it would be better to increase the

112   engine's transient power response to use gasoline, which has a relatively low heat of vaporisation.

113   With the advantages of low carbon content, ethanol is normally recognised as reducing the production

114   of PM emissions during engine combustion process [28][29][30].

115
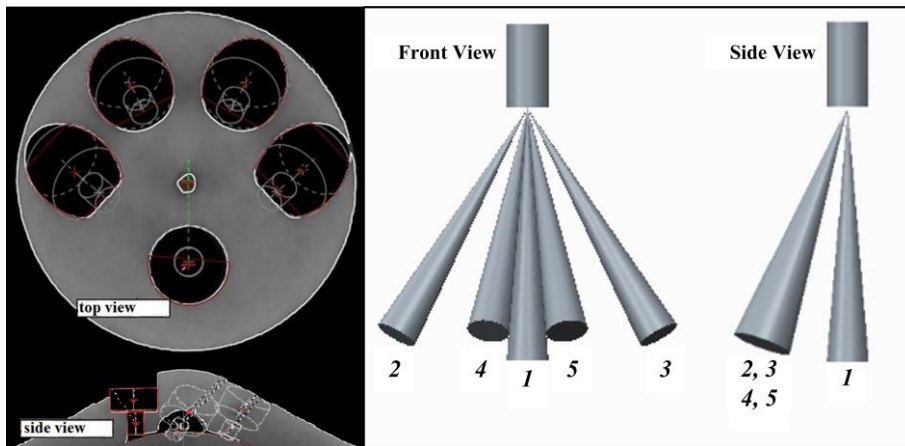
117   **Fig. 1.** The orifice geometry and spray sketch of the GDI injector used in this investigation

118

119   **Table 1.** Fuel properties of gasoline and ethanol

| Fuel type	Gasoline	Ethanol
Chemical formula	C5-C12	C_2H_5OH
Relative molecular mass	95-120	46
Gravimetric oxygen content (%)	< 1	34.78
Research octane number	95	107
Density (293 K) (kg/L)	0.73	0.789
Kinematic viscosity (293 K) (mm^2/s)	0.71	1.52
Surface tension (293 K) (mN/m)	22	21.97
Boiling range (K)	303-473	351
Low heating value (kJ/kg)	44300	26900
Latent heat of vaporisation (kJ/kg)	370	840
Laminar flame speed (293 K) (m/s)	0.33	0.5
Stoichiometric air-fuel ratio	14.7	8.95

The comparative investigation on the macroscopic characteristics of gasoline and ethanol impingement spray was carried out via Schlieren technique, which has the advantage of getting the image of gas-liquid two-phase based on the differences of refractive index gradients [33][34][35]. The whole experimental setup of macroscopic characteristics can be seen in Fig. 2. After connecting to a metal holder, injector can be adjusted and fixed to a specific distance and angle referring to a wall, which is a very flat aluminium alloy plate with a roughness of less than 0.4 mm.

Fuel injection pressure was selected to be 10 MPa, 30 MPa and 50 MPa, representing common, high and ultra-high pressures of GDI injector, respectively. The drive signal of fuel injection was transmitted from a programmable Electronic Control Unit (ECU), which could also synchronise injection with "768 × 768 pixels at 10000 frames per second" images captured by a high-speed camera. Then, using MATLAB, the captured images were converted to grayscale, followed by image processing and calculation. In order to minimise the potential interference of suspended fuel droplets caused by the preceding injection, injection pulse width was set to be 1.2 ms, and the injection frequency was fixed to be a very low level of 0.1 Hz. The aluminium alloy plate was cleaned and restored thoroughly every five injections. Fuel was injected into an ambient condition of 293 ± 0.5 K and 0.1 MPa. An air extractor was used to eliminate the safety risks of experimental site. Besides, each condition should be repeated thirty times during the test to improve the measurement accuracy.

As shown in Fig. 3, based on the design of side-mounted injector of engine, injector's orientation was set to be in an inclined direction in this investigation. The jets "2" to "5" hit the wall vertically, whilst jet "1" hits the wall at an inclined angle. The wall was located at a distance of 33 mm from the tip of injector. Moreover, to characterise the spray development and atomisation process from a macroscopic view, the parameterisation of impingement spray propagation is quite helpful and

142   scientific. Therefore, some important parameters were introduced in this investigation. According to

143   a reference line that is perpendicular from the injector top to the wall, H_N and H_F denote rebound

144   height of the near side and far side for impingement spray, respectively. D_N and D_F each denote

145   diffusion distance of the near side and far side. A_S denotes area of impingement spray. P_I denotes

146   fuel injection pressure; t denotes time After Start of fuel Injection (ASOI).

147
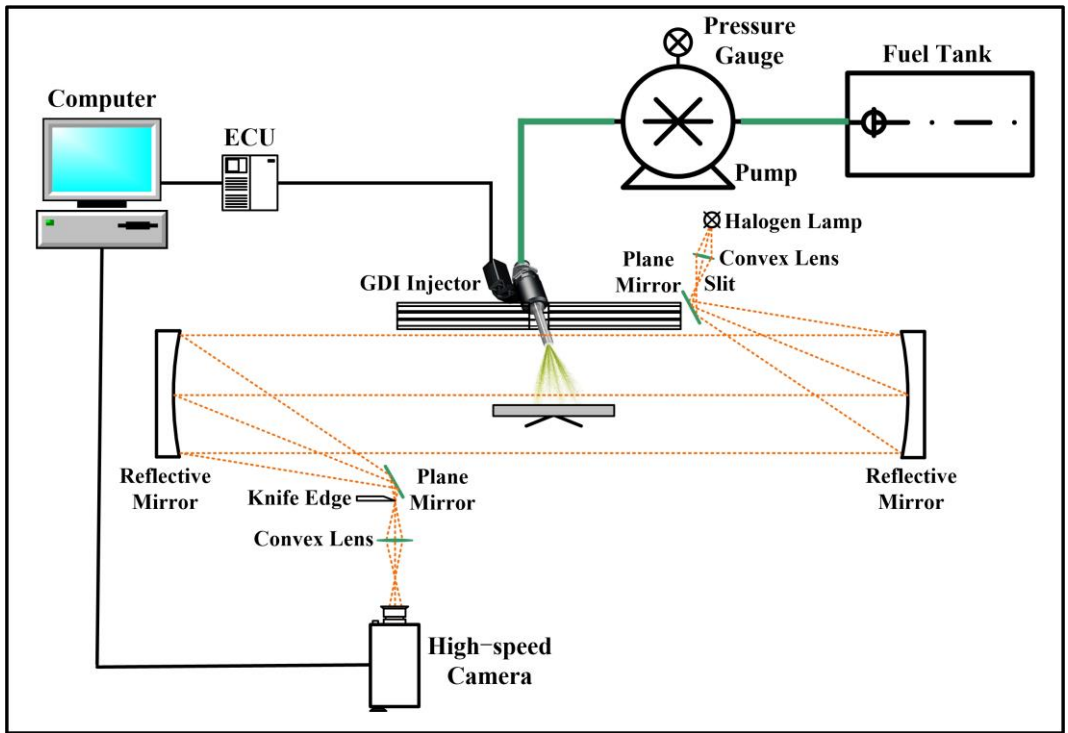
Fig. 2. Experimental setup of macroscopic impingement spray characteristics
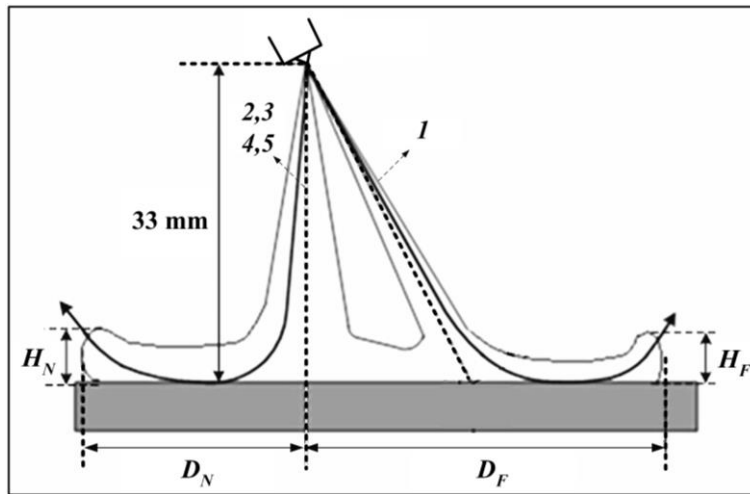
Fig. 3. Determination of parameters for macroscopic impingement spray characteristics
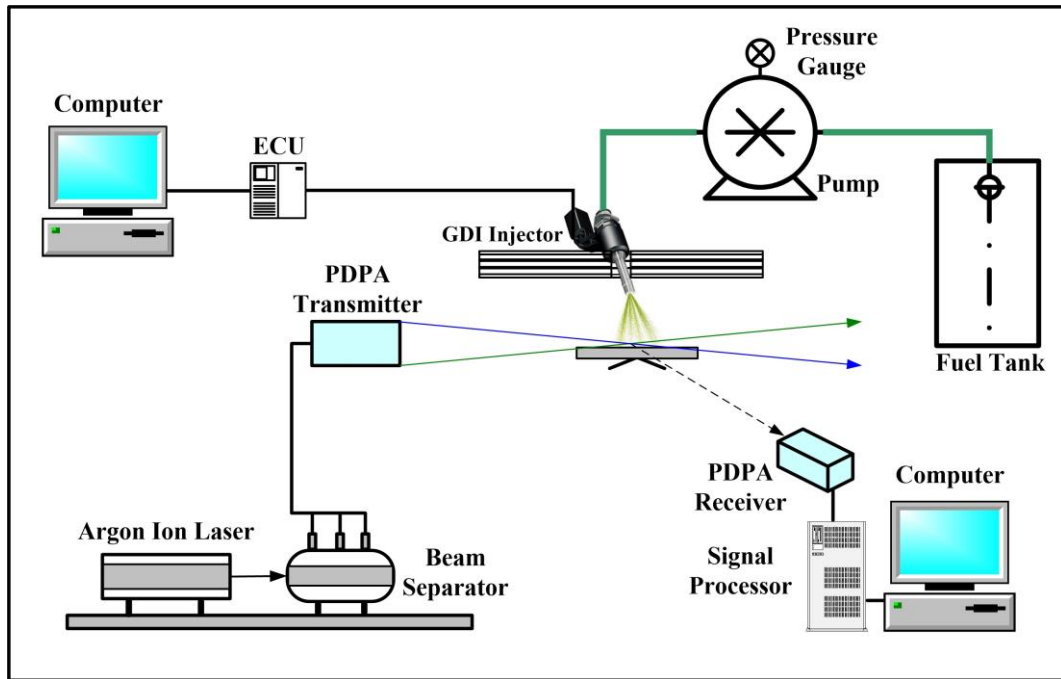
2.2. Experimental setup and procedures of microscopic spray characteristics

Regarding the investigation of microscopic characteristics of gasoline and ethanol impingement spray, the experimental setup mainly based on a Phase Doppler Particles Analyser (PDPA) system can be seen in Fig. 4.

Using a 1.3 W power argon-ion laser and a 180 MHz signal processor of the PDPA system, the measuring range of droplet velocity was set to be -151.95 to 238.77 m/s with 0.01 m/s resolution. Meantime, the measurement of droplet diameter ranges from 0 to 236 μm with 0.1 μm. As shown in Fig. 5, two measurement points ("A" and "B") were selected at 4 mm above the wall. Point "A" was at the axis of injector, representing droplet behaviour in the central region of jet "1". To better understand the droplet behaviour of impingement spray's evolution, Point "B" was chosen at 10 mm to the right of Point "A". Besides, in the PDPA test, D_d denotes droplet diameter; D_{SMD} denotes Sauter mean diameter of droplets; D_{sub} denotes the difference of D_{SMD} between the conditions P_I = 10 MPa and other P_I (30 MPa, 50 MPa). p_d denotes probability. V_N denotes average normal component of droplet velocity; V_T denotes average tangential component of droplet velocity. The positive direction of V_N and V_T was also defined as shown in Fig. 5.

For each test condition, in order to guarantee the measurement accuracy, data collection and analysis were from 20000 validated droplets, and the measurement should be repeated three times. The other experimental conditions and rules of microscopic characteristics investigation are the same with those of macroscopic characteristics.

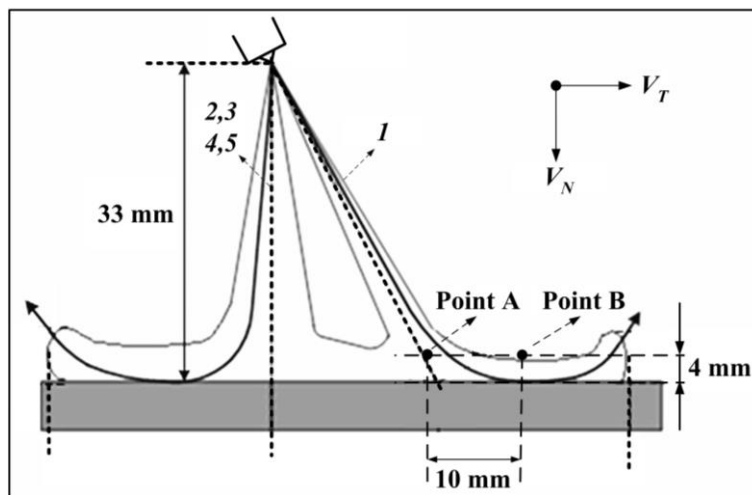**Fig. 4.** Experimental setup of microscopic impingement spray characteristic

Fig. 5. PDPA measurement points of microscopic impingement spray characteristic

3. Results and discussion

3.1. Macroscopic characteristics of gasoline and ethanol impingement spray

In order to completely understand the macroscopic characteristics, this section shows the results of H_N, H_F, D_N, D_F and A_S for both gasoline and ethanol with varying P_I. The maximum statistical time of the figures in this section is 3.0 ms ASOI, which is attributed to two factors. First, as the fuel injection pulse width was 1.2 ms, 3.0 ms ASOI can fully cover the relatively long time

182   after the end of fuel injection. Second, the curves' trends in the figures are relatively stable near 3.0

183   ms ASOI and do not have apparent changes again.

184   In addition, the percentage changes in the figures of this section mean the change of gasoline

185   concerning ethanol at the end of the statistical time. It shows the result of "the difference between the

186   value of gasoline over ethanol" divided by "the value of ethanol" in percentage.

187   As H_N shown in Fig. 6, the t of reaching field boundary is advanced from around 2.8 ms ASOI

188   to around 1.7 ms ASOI with the increase of P_I from 10 MPa to 30 MPa. Then, the corresponding t

189   would be further advanced to 1.3 ms ASOI by increasing P_I to 50 MPa. Regarding H_F of 3.0 ms

190   ASOI shown in Fig. 7, it improves from around 18 mm to around 27.3 mm by increasing P_I from

191   10 MPa to 50 MPa. This is mainly because under higher P_I, the kinetic energy of spray droplets can

192   be improved owing to the higher initial velocity. Based on the energy conservation law, the sum of

193   droplets' kinetic energy and surface energy can be converted to energy dissipation and surface energy

194   during the impingement process. Hence, the energy of rebound and splash for the droplets is enhanced,

195   increasing the growth rate of H_N and H_F. This would help promote the mixing of gasoline and air,

196   reducing the possibility of PM emissions in GDI engines.

197   In addition, Fig.6 and Fig. 7 demonstrate that under the same P_I, H_N and H_F of gasoline are a

198   bit higher than those of ethanol. This can mainly be attributed to the difference in fuel properties

199   between gasoline and ethanol. In the same condition of P_I and height, initial velocity of droplets

200   would be reduced with a higher fluid density according to Bernoulli's principle stated in Equation (1).

201   Hence, compared to ethanol, the initial velocity of gasoline spray is higher owing to the lower fluid

202   density.

$$\frac{1}{2}\rho_L v^2 + \rho_L gz + P = C \tag{1}$$

Here, ρ_L and v is the mass density and flow velocity of the fluid, respectively. g is the acceleration of gravity; z is the height of a location above a reference plane; P is pressure at the chosen point; C denotes constant.
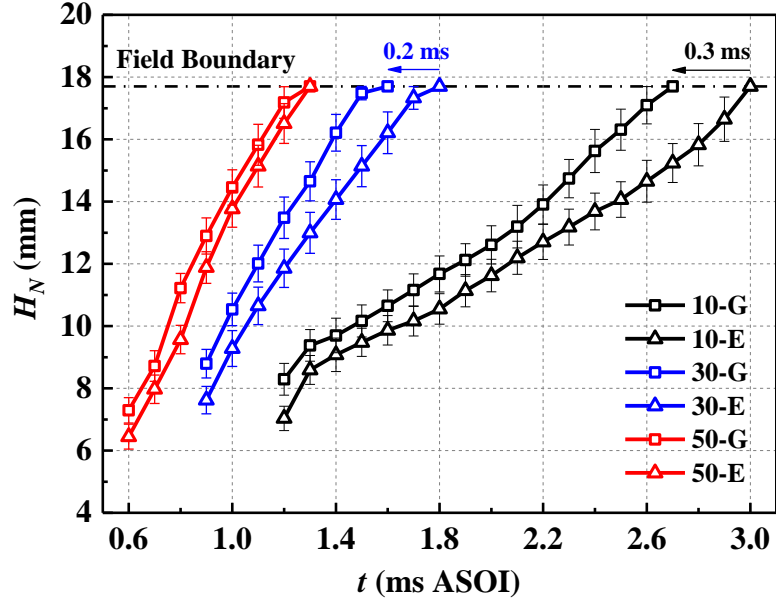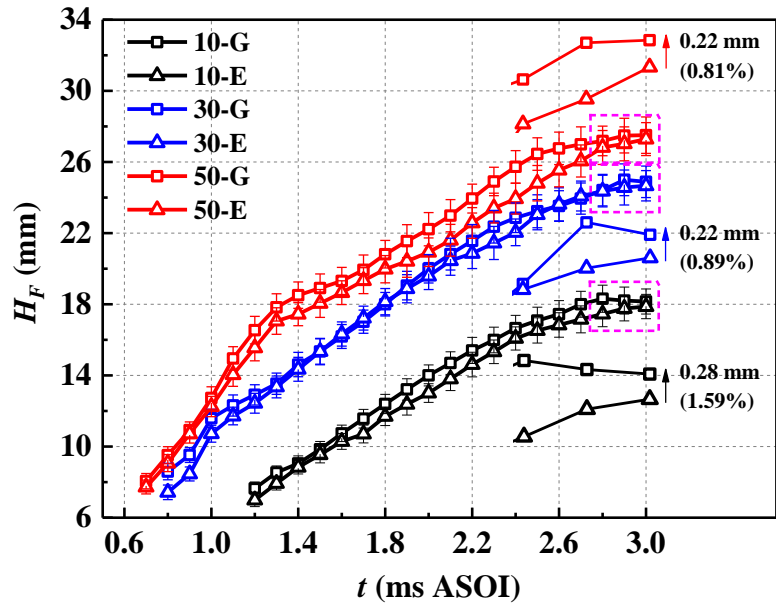

Fig. 6. H_N of gasoline and ethanol impingement spray with varying P_I
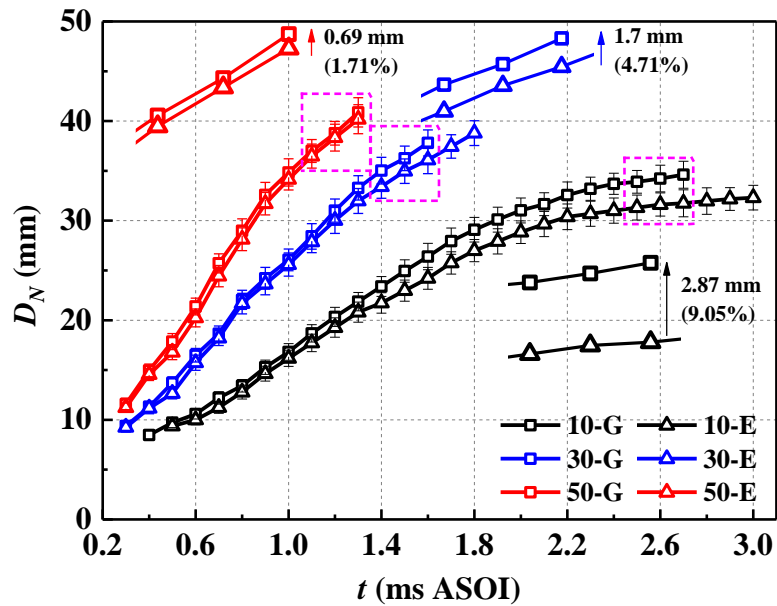

Fig. 7. H_F of gasoline and ethanol impingement spray with varying P_I

213 Fig. 8 and Fig. 9 present D_N and D_F of gasoline and ethanol with varying P_I. It can be seen

214 that with the increase of P_I from 10 MPa to 50 MPa, the difference in D_N between gasoline and

215 ethanol is greatly reduced. Especially under $P_I = 50$ MPa, D_N of gasoline is only 0.69 mm or 1.71%

216 higher than that of ethanol at 1.3 ms ASOI, which is the t of reaching field boundary for H_N. With

217 regards to D_F of gasoline, it is 0.27 mm or 0.45% higher than that of ethanol at 3.0 ms ASOI under

218 $P_I = 10$ MPa. However, when P_I increases to 30 MPa and 50 MPa, D_F of gasoline becomes weaker,

219 which is 1.81 mm and 2.9 mm lower than ethanol at 3.0 ms ASOI. This is mainly because the vortices

220 around the boundary of gasoline impingement spray are a little stronger than ethanol, as shown in Fig.

221 10. The stronger vortices would have a negative effect on the growth of D_F, owing to the increased

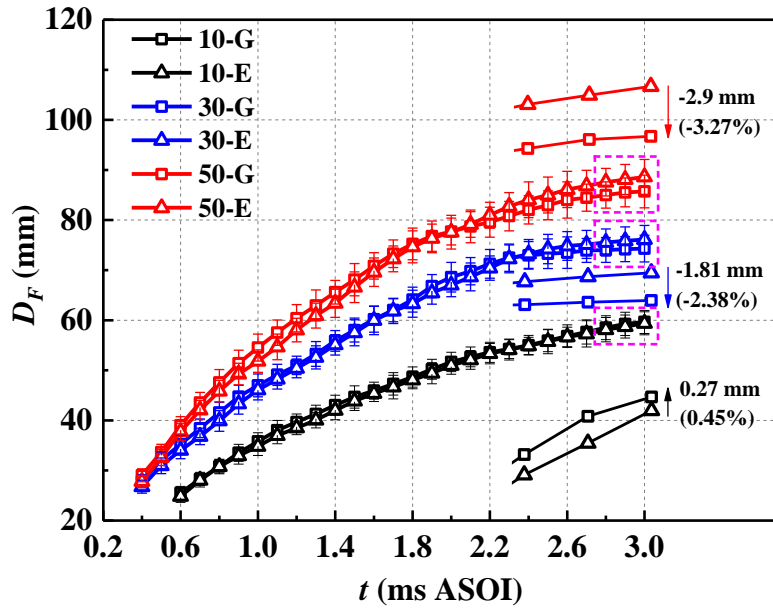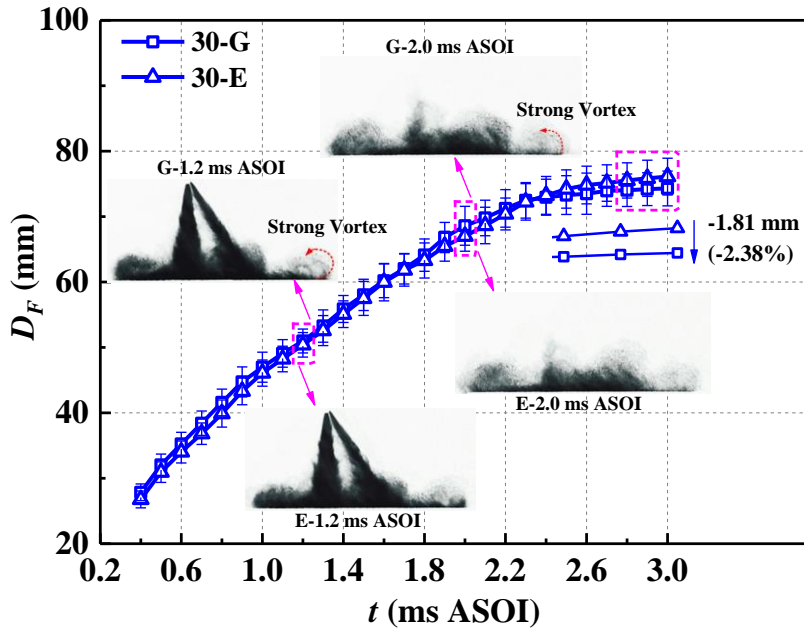222 kinetic energy for droplets moving toward inner inside of spray.

223

Fig. 8. D_N of gasoline and ethanol impingement spray with varying P_I

226

Fig. 9. D_F of gasoline and ethanol impingement spray with varying P_I

228

Fig. 10. Comparison between gasoline and ethanol spray under P_I = 30 MPa

230

Fig. 11 shows A_S of gasoline and ethanol under different P_I. For both gasoline and ethanol, the

overall trend of A_S is ascending with the increase of P_I. It indicates that the spread of fuel spray

could be further prompted under high P_I, thus it would be beneficial to enhance the air-fuel mixture

homogeneity for GDI engines. Moreover, the comparison between gasoline and ethanol is quite different. Under P_I = 10 MPa, A_S of gasoline is slightly higher than ethanol, which is 1303.93 mm^2 and 1300.91 mm^2 at 3.0 ms ASOI, respectively. Under higher P_I, A_S of gasoline is gradually exceeded by of ethanol as time progresses. At 3.0 ms ASOI, A_S of gasoline is 2.34% and 3.05% lower than ethanol under P_I = 30 MPa and P_I = 50 MPa, respectively. This is due to a combined impact of two reasons. One is that compared to ethanol, stronger vortices around the boundary enhance the kinetic energy for droplets moving toward inner inside of spray, which could slow down the growth of A_S. The other reason can be attributed to the lower kinematic viscosity of gasoline. As shown in Equation (2), a larger Re could enhance the instability of gasoline impingement spray, increasing violent breakup and negative effects on the A_S expansion.

$$Re = \frac{UD_d}{v} \tag{2}$$

Here, Re is Reynolds number; U, D_d and v are each normal incident velocity, droplet diameter and kinetic viscosity.
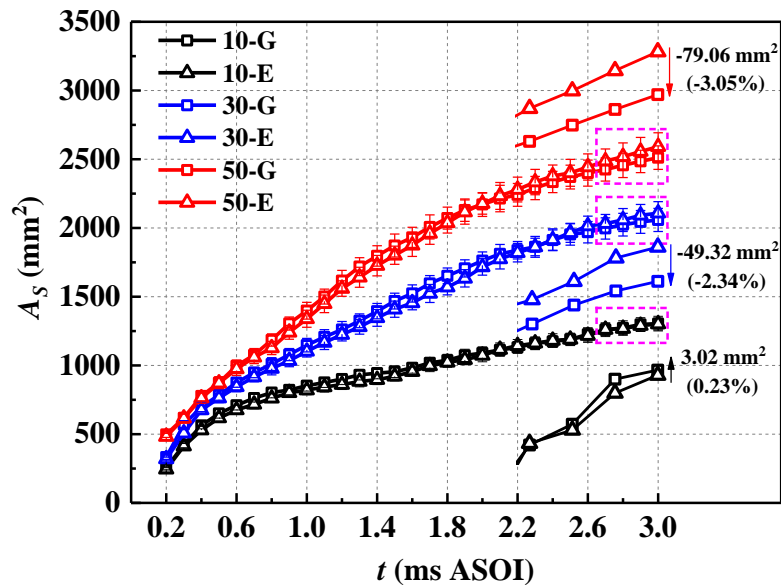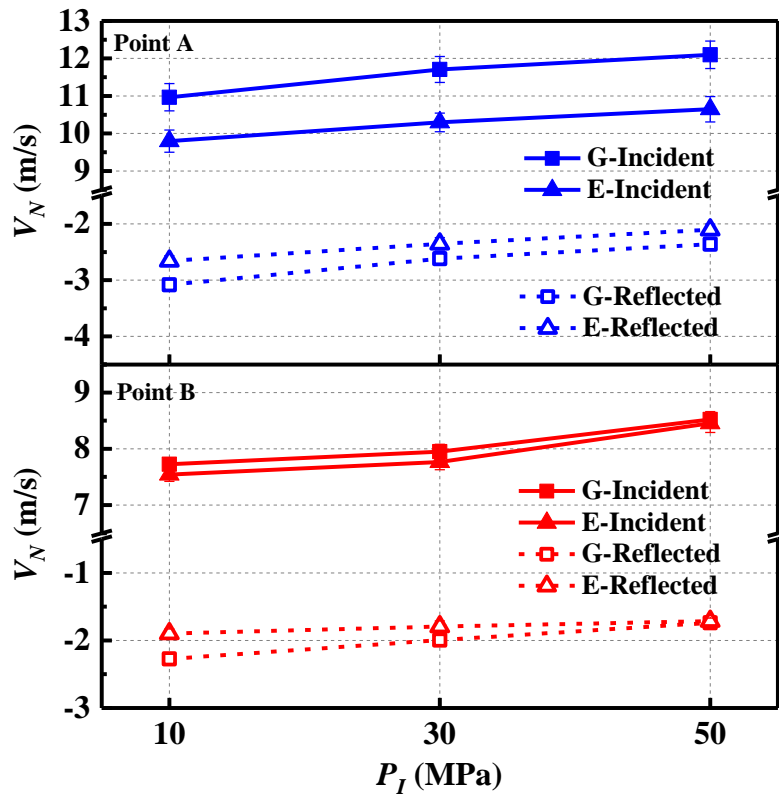

Fig. 11. A_S of gasoline and ethanol impingement spray with varying P_I

3.2. Microscopic characteristics of gasoline and ethanol impingement spray

Fig. 12 and Fig. 13 present V_N and V_T at points "A" and "B" of gasoline and ethanol. It can be seen that the overall trends of V_N and V_T are generally stable by increasing P_I, but the changes of incident droplets and reflected droplets are a bit different. With the increase of P_I from 10 MPa to 50 MPa, V_N and V_T of incident droplets increase by around 1 m/s for both "A" and "B". However, there is a slight decrease in the absolute value of V_N and V_T of reflected droplets in the meantime. This is largely because that by increasing P_I, it would be easier for droplets to break down after impingement, increasing irregularity in the direction of reflected droplets' movement. In addition, due to higher initial velocity of gasoline impingement spray, the absolute value of V_N and V_T of gasoline is a bit higher than ethanol under the same P_I. However, with the increase of P_I, the difference in velocity between gasoline and ethanol becomes very slight at "B", which is similar to the corresponding variations and characteristics of D_N and D_F in Fig. 8 and Fig. 9.
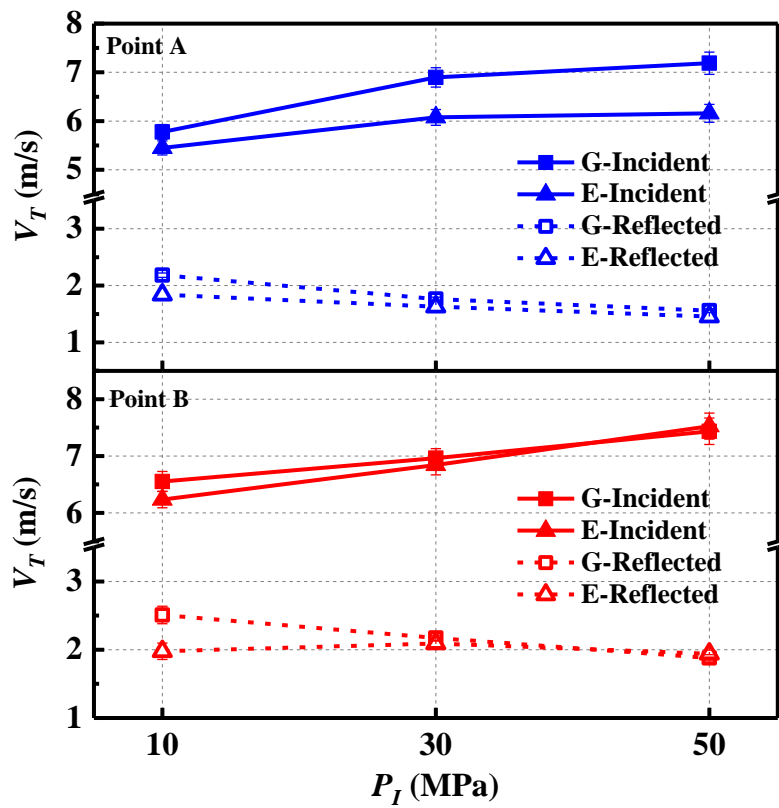
263

Fig. 12. V_N at points "A" and "B" of gasoline and ethanol impingement spray with varying P_I

265

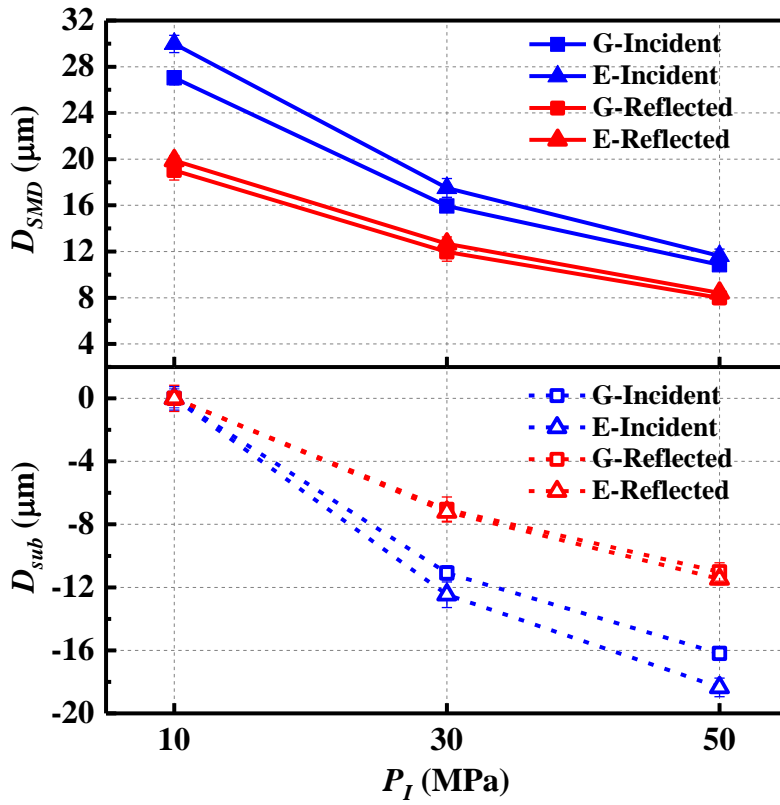**Fig. 13.** V_T at points "A" and "B" of gasoline and ethanol impingement spray with varying P_I

267   Regarding the droplet size of "A" and "B", two main features can be found in Fig. 14 and Fig. 15,

268   which present both D_{SMD} and D_{Sub} of gasoline and ethanol. First, with the increase of P_I from 10

269   MPa to 50 MPa, D_{SMD} presents a significant decreasing trend at both "A" and "B". For incident

270   droplets, D_{SMD} decreases from around 28 μm to around 10 μm. Meantime, D_{SMD} decreases from

271   around 18 μm to around 8 μm for reflected droplets. Second, under the same P_I, a smaller D_{SMD} can

272   be seen for the gasoline impingement spray compared to ethanol. These features can be further

273   explained by p_d of D_d. For example, from p_d of D_d of incident droplets at "A" shown in Fig. 16,

274   it can be observed that compared to P_I = 10 MPa, the centralisation of D_d moves towards smaller

275   size under P_I = 50 MPa. The p_d of D_d above 20 μm decreases significantly to close to 0% under

276   P_I = 50 MPa. Moreover, a bit higher p_d of small D_d can be found in gasoline compared to ethanol.

277   The reason of these features can be attributed to that increasing P_I would promote the spray breakup

278   progress and produce a larger number of tiny droplets. Compared to low P_I, high P_I could easily

279   lead to better air-fuel mixture homogeneity, contributing to mitigate PM emissions from GDI engines.

280   Besides, the larger Re of gasoline further increases the level of spray instability and breakup, leading

281   to a better air-fuel mixture quality compared to ethanol.
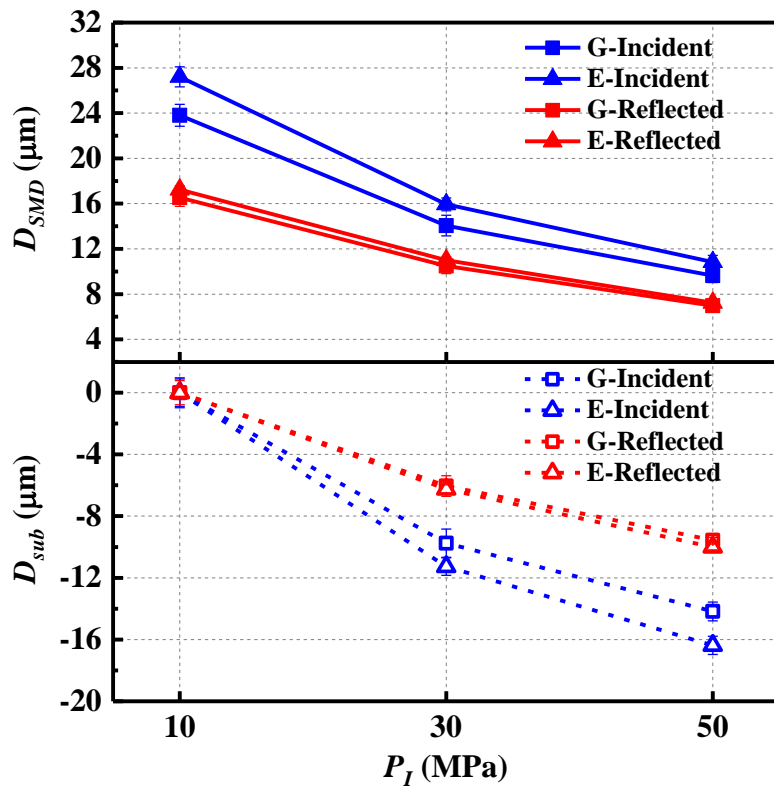
282

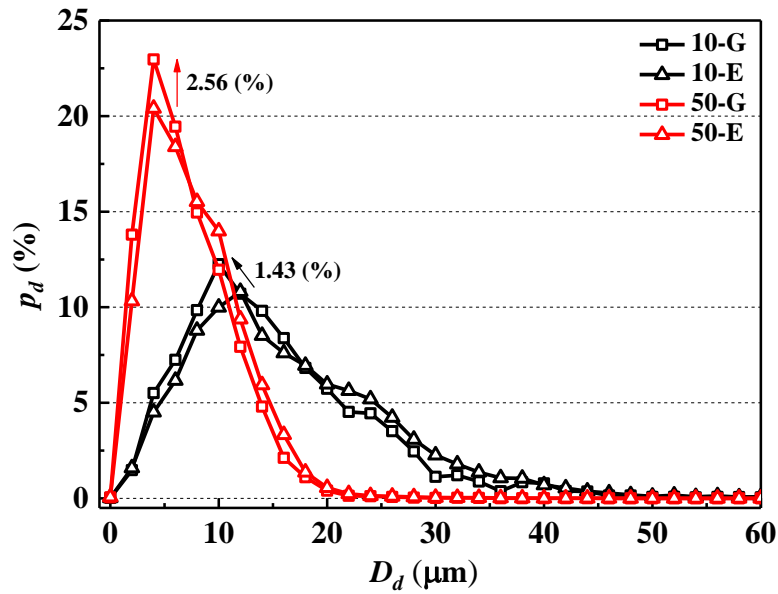**Fig. 14.** D_{SMD} and D_{sub} at point "A" of gasoline and ethanol impingement spray with varying P_I

Fig. 15. D_{SMD} and D_{sub} at point "B" of gasoline and ethanol impingement spray with varying P_I

Fig. 16. p_d of D_d of incident droplets at point "A" of gasoline and ethanol impingement spray with varying P_I

4. Conclusions

An investigation was conducted to explore and compare the macroscopic and microscopic characteristics of gasoline and ethanol impingement spray from a GDI injector under injection pressure up to 50 MPa. This investigation provides theoretical perspectives for understanding impingement spray characteristics, which also benefits the model mechanisms establishment in numerical work. In the meantime, the investigation's findings could contribute to forming a more homogeneous air-fuel mixture in GDI engines, further reducing PM emissions. The main conclusions can be summarised as follows:

(1) Compared to ethanol, H_N and H_F of gasoline are a bit higher under the same P_I. By increasing P_I to 50 MPa, the difference in D_N between gasoline and ethanol is greatly reduced. Meantime, D_F of gasoline becomes lower than ethanol at 3.0 ms ASOI.

(2) With the increase of P_I, the overall trend of A_S is ascending for both gasoline and ethanol. As time progresses, A_S of gasoline is gradually exceeded by ethanol under P_I = 30 MPa

302   and $P_I = 50$ MPa.

303   (3) For both gasoline and ethanol, with the increase of P_I from 10 MPa to 50 MPa, V_N and V_T

304   of incident droplets increase by around 1 m/s. Meantime, there is a slight decrease in the

305   absolute value of V_N and V_T of reflected droplets.

306   (4) Compared to ethanol, a smaller D_{SMD} can be seen for the gasoline impingement spray under

307   the same P_I. By increasing P_I from 10 MPa to 50 MPa, D_{SMD} decreases from around 28

308   µm to around 10 µm for incident droplets. Meantime, D_{SMD} decreases from around 18 µm

309   to around 8 µm for reflected droplets.

310   In addition, to further establish the new framework about impingement spray characteristics of

311   gasoline and ethanol from a GDI injector under high injection pressure. In future work, the effects of

312   many other helpful injection parameters on impingement spray characteristics can be explored, such

313   as injection duration, distance, angle, pulse frequency, etc.

314

315   **CRediT authorship contribution statement**

316   **Xiang Li:** Conceptualization, Methodology, Formal analysis, Investigation, Data curation,

317   Visualization, Writing - original draft. **Pavlos Dimitriou:** Writing - reviewing & editing. **Dayou Li:**

318   Writing - reviewing & editing. **Tahmina Ajmal**: Project administration. **Abdel Aitouche**: Project

319   administration, Funding acquisition. **Raouf Mobasheri**: Project administration. **Oyuna Rybdylova:**

320   Writing - reviewing & editing. **Yiqiang Pei**: Methodology, Project administration, Funding

321   acquisition. **Zhijun Peng:** Methodology.

322

Reference

[1] Hughes, D.D., Christiansen, M.B., Milani, A., Vermeuel, M.P., Novak, G.A., Alwe, H.D., Dickens, A.F., Pierce, R.B., Millet, D.B., Bertram, T.H., Stanier, C.O., 2021. PM2. 5 chemistry, organosulfates, and secondary organic aerosol during the 2017 Lake Michigan Ozone Study. Atmos. Environ. 244, 117939.

[2] Zhang, Y., Lou, D., Tan, P., Hu, Z., Fang, L., 2022. Effect of SCR downsizing and ammonia slip catalyst coating on the emissions from a heavy-duty diesel engine. Energy Rep. 8, 749-757.

[3] Manisalidis, I., Stavropoulou, E., Stavropoulos, A., Bezirtzoglou, E., 2020. Environmental and health impacts of air pollution: a review. Frontiers in public health 14.

[4] Guo, J., Jiang, Y., Yu, Y., Liu, W., 2020. A novel energy consumption prediction model with combination of road information and driving style of BEVs. Sustainable Energy Technologies and Assessments 42, 100826.

[5] İnci, M., Büyük, M., Demir, M.H., İlbey, G., 2021. A review and research on fuel cell electric vehicles: Topologies, power electronic converters, energy management methods, technical challenges, marketing and future aspects. Renewable Sustainable Energy Rev. 137, 110648.

[6] Attar, M.A., Herfatmanesh, M.R., Zhao, H., Cairns, A., 2014. Experimental investigation of direct injection charge cooling in optical GDI engine using tracer-based PLIF technique. Exp. Therm. Fluid Sci. 59, 96-108.

[7] Luo, H., Nishida, K., Uchitomi, S., Ogata, Y., Zhang, W., Fujikawa, T., 2020. Effect of spray impingement distance on piston top fuel adhesion in direct injection gasoline engines. Int. J. Engine Res. 21(5), 742-754.

[8] Chen, Z., Wei, X., Zhang, Y., He, T., Zhang, Q., 2019. Combined impact of n-butanol additive and spark timing on combustion and efficiency of a GDI engine. J. Energy Eng. 145(5), 04019018.

352 [9] Li, X., Pei, Y., Li, D., Ajmal, T., Aitouche, A., Mobasheri, R., Peng, Z., 2021. Implementation of oxy-fuel
353   combustion (OFC) technology in a gasoline direct injection (GDI) engine fueled with gasoline–ethanol blends.
354   ACS omega 6(44), 29394-29402.

355 [10] Wang, L., Hong, C., Li, X., Yang, Z., Guo, S., Li, Q., 2022. Review on blended hydrogen-fuel internal
356   combustion engines: A case study for China. Energy Rep. 8, 6480-6498.

357 [11] Chang, M., Yu, Y.S., Park, S., Park, S., 2022. Spray dynamics and atomization characteristics of multi-hole
358   GDI injectors under flash boiling conditions. Appl. Therm. Eng. 200, 117626.

359 [12] Giechaskiel, B., Joshi, A., Ntziachristos, L., Dilara, P., 2019. European regulatory framework and particulate
360   matter emissions of gasoline light-duty vehicles: A review. Catalysts 9(7), 586.

361 [13] Awad, O.I., Ma, X., Kamil, M., Ali, O.M., Zhang, Z., Shuai, S., 2020. Particulate emissions from gasoline direct
362   injection engines: A review of how current emission regulations are being met by automobile manufacturers.
363   Sci. Total Environ. 718, 137302.

364 [14] Li, X., Li, D., Pei, Y., Peng, Z., 2022. Optimising microscopic spray characteristics and particle emissions in a
365   dual-injection spark ignition (SI) engine by changing GDI injection pressure. Int. J. Engine Res.
366   14680874221082793.

367 [15] Eitel, F., Schäfer, J., Königstein, A., Heeger, C., 2018. Fuel Pressure Increase up to 50 MPa for Gasoline Direct-
368   injection Engines. MTZ worldw. 79(7), 50-55.

369 [16] Husted, H., Spegar, T.D., Spakowski, J., 2014. The effects of GDI fuel pressure on fuel economy (No. 2014-
370   01-1438). SAE Technical Paper.

371 [17] Kim, T., Song, J., Park, J., Park, S., 2018. Numerical and experimental study on effects of fuel injection timings
372   on combustion and emission characteristics of a direct-injection spark-ignition gasoline engine with a 50 MPa
373   fuel injection system. Appl. Therm. Eng. 144, 890-900.

374 [18] Lee, Z., Park, S., 2020. Particulate and gaseous emissions from a direct-injection spark ignition engine fueled
375   with bioethanol and gasoline blends at ultra-high injection pressure. Renewable Energy 149, 80-90.

376 [19] Lou, D., Wang, T., Fang, L., Tan, P., Hu, Z., Zhang, Y., Xu, Z., Cheng, C., Wang, S., Zhang, Y., 2022.
377   Investigation of the combustion and particle emission characteristics of a GDI engine with a 50 MPa injection
378   system. Fuel 315, 123079.

379 [20] Li, X., Pei, Y.Q., Qin, J., Zhang, D., Wang, K. and Xu, B., 2018. Effect of ultra-high injection pressure up to
380   50 MPa on macroscopic spray characteristics of a multi-hole gasoline direct injection injector fueled with
381   ethanol. Proc. Inst. Mech. Eng., Part D 232(8), 1092-1104.

382 [21] Luo, H., Nishida, K., Ogata, Y., Zhang, W., 2021. Microscopic characteristics of near-nozzle spray at the initial
383   and end stages. Fuel 283, 118953.

384 [22] Chang, F., Luo, H., Zhan, C., Nishida, K., Ogata, Y., 2021. Droplets velocity and diameter variations of wall
385   impinging spray created by slicer. Fuel 299, 120894.

386 [23] Zhang, G., Luo, H., Kita, K., Ogata, Y., Nishida, K., 2022. Statistical variation analysis of fuel spray
387   characteristics under cross-flow conditions. Fuel 307, 121887.

388 [24] Montanaro, A., Allocca, L., Meccariello, G., 2020. Effects of Ultra-High Injection Pressures up to 100 MPa on
389   Gasoline Spray Morphology (No. 2020-01-0320). SAE Technical Paper.

390   [25] Migliaccio, M., Montanaro, A., Lucchini, T., Allocca, L., Paredi, D., 2020. Numerical investigation on GDI
391   spray under high injection pressure up to 100 MPa (No. 2020-01-2108). SAE Technical Paper.

392   [26] Huang, H., Li, Z., Teng, W., Huang, R., Liu, Q., Wang, Y., 2019. Effects of EGR rates on combustion and
393   emission characteristics in a diesel engine with n-butanol/PODE3-4/diesel blends. Appl. Therm. Eng. 146, 212-
394   222.

395   [27] Huang, H., Li, Z., Teng, W., Zhou, C., Huang, R., Liu, H., Pan, M., 2019. Influence of n-butanol-diesel-PODE3-
396   4 fuels coupled pilot injection strategy on combustion and emission characteristics of diesel engine. Fuel 236,
397   313-324.

398   [28] Zhuang, Y., Ma, Y., Qian, Y., Teng, Q., Wang, C., 2020. Effects of ethanol injection strategies on mixture
399   formation and combustion process in an ethanol direct injection (EDI) plus gasoline port injection (GPI) spark-
400   ignition engine. Fuel 268, 117346.

401   [29] Puricelli, S., Cardellini, G., Casadei, S., Faedo, D., Van den Oever, A.E.M., Grosso, M., 2021. A review on
402   biofuels for light-duty vehicles in Europe. Renewable Sustainable Energy Rev. 137, 110398.

403   [30] Li, X., Pei, Y., Ajmal, T., Rana, K.J., Aitouche, A., Mobasheri, R., Peng, Z., 2021. Numerical investigation on
404   implementing Oxy-Fuel Combustion (OFC) in an ethanol-gasoline Dual-Fuel Spark Ignition (DFSI) engine.
405   Fuel 302, 121162.

406   [31] Badawy, T., Xu, H., Li, Y., 2022. Macroscopic spray characteristics of iso-octane, ethanol, gasoline and
407   methanol from a multi-hole injector under flash boiling conditions. Fuel 307, 121820.

408   [32] Badawy, T., Mansour, M.S., Daabo, A.M., Aziz, M.M.A., Othman, A.A., Barsoum, F., Basouni, M., Hussien,
409   M., Ghareeb, M., Hamza, M., Wang, C., 2021. Selection of second-generation crop for biodiesel extraction and
410   testing its impact with nano additives on diesel engine performance and emissions. Energy 237, 121605.

411   [33] Allocca, L., Lazzaro, M., Meccariello, G., Montanaro, A., 2016. Schlieren visualization of a GDI spray
412   impacting on a heated wall: Non-vaporizing and vaporizing evolutions. Energy 108, 93-98.

413   [34] Wu, J., Kang, Z., Zhang, Z., Li, Z., Deng, J., Wu, Z., 2018. Effects of Vessel and Water Temperatures on Direct
414   Injection in Internal Combustion Rankine Cycle Engines. Automot. Innovation 1(4), 331-341.

415   [35] Li, F., Lee, C.F., Wu, H., Wang, Z., Liu, F., 2019. An optical investigation on spray macroscopic characteristics
416   of ducted fuel injection. Exp. Therm. Fluid Sci. 109, 109918.

417

Appendix

419   *Nomenclature*

ASOI	After Start of Injection
BEV	Battery Electric Vehicle
ECU	Electronic Control Unit
EGR	Exhaust Gas Recirculation
FCEV	Fuel Cell Electric Vehicle
GDI	Gasoline Direct Injection
ICE	Internal Combustion Engine

PDPA	Phase Doppler Particles Analyser
PFI	Port Fuel Injection
PM	Particulate Matter
SI	Spark Ignition
P_I	Injection Pressure
A_S	Spray Area
H_N	Rebound Height of the Near Side
H_F	Rebound Height of the Far Side
D_N	Diffusion Distance of the Near Side
D_F	Diffusion Distance of the Far Side
V_N	Average Normal Component of Droplet Velocity
V_T	Average Tangential Component of Droplet Velocity
p_d	Probability
t	Time After Start of Fuel Injection
D_d	Droplet Diameter
D_{SMD}	Sauter Mean Diameter of Droplets
D_{sub}	Difference of D_{SMD} between P_I = 10 MPa and other P_I

420